Key Points:
- Equilibrium climate sensitivity (ECS) decreases with increasing forcing in 12 out of 15 Earth system models of intermediate complexity (EMICs)
- In one such EMIC, this ECS state-dependence is mainly due to declining sea ice-albedo feedback in the Southern Ocean
- Ocean mixing adjustments can delay the emergence of state-dependence by multiple centuries

Supporting Information:
- Supporting Information S1

Correspondence to:
P. L. Pfister,
pfister@climate.unibe.ch

State-Dependence of the Climate Sensitivity in Earth System Models of Intermediate Complexity

Patrik L. Pfister[1,2] (ID) **and Thomas F. Stocker**[1,2] (ID)

[1]Climate and Environmental Physics, Physics Institute, University of Bern, Bern, Switzerland, [2]Oeschger Center for Climate Change Research, University of Bern, Bern, Switzerland

Abstract Growing evidence from general circulation models (GCMs) indicates that the equilibrium climate sensitivity (ECS) depends on the magnitude of forcing, which is commonly referred to as state-dependence. We present a comprehensive assessment of ECS state-dependence in Earth system models of intermediate complexity (EMICs) by analyzing millennial simulations with sustained $2\times CO_2$ and $4\times CO_2$ forcings. We compare different extrapolation methods and show that ECS is smaller in the higher-forcing scenario in 12 out of 15 EMICs, in contrast to the opposite behavior reported from GCMs. In one such EMIC, the Bern3D-LPX model, this state-dependence is mainly due to the weakening sea ice-albedo feedback in the Southern Ocean, which depends on model configuration. Due to ocean-mixing adjustments, state-dependence is only detected hundreds of years after the abrupt forcing, highlighting the need for long model integrations. Adjustments to feedback parametrizations of EMICs may be necessary if GCM intercomparisons confirm an opposite state-dependence.

1. Introduction

The equilibrium climate sensitivity (ECS), defined as the equilibrium global mean temperature response to a doubling of atmospheric CO_2, is a useful metric for climate model intercomparison and data-based projections (Charney et al., 1979; Intergovernmental Panel on Climate Change (IPCC), 2013). ECS is determined by the combined strength of various climate feedbacks, which are physical processes acting to amplify or dampen temperature perturbations (ΔT) caused by radiative forcing (R). In a global energy balance model (EBM) (Gregory et al., 2004), these processes are represented by a feedback parameter λ (in Wm^{-2} K^{-1}):

$$R - N = -\lambda \Delta T, \tag{1}$$

where N is the energy imbalance at the top of the atmosphere (TOA), that is, the planetary heat uptake. The equilibrium temperature anomaly (ΔT_{eq}) is reached once energy balance is restored in the perturbed climate state ($N = 0$): $\Delta T_{eq} = -R/\lambda_{eq}$. The equilibrium feedback parameter λ_{eq} may differ from the transient feedback parameter λ (Andrews et al., 2015; Armour et al., 2013; Geoffroy et al., 2013; Gregory et al., 2015; Knutti & Rugenstein, 2015; Winton et al., 2010). This study focuses on the complementary question whether λ_{eq} itself is state dependent. State-dependence is used synonymously with forcing dependence here, as a different forcing generally enables a different climate state — including differences in temperature, ocean circulation, radiative properties, and related variables. ECS state-dependence is equivalent to λ_{eq} state-dependence, as ECS can be estimated by scaling any ΔT_{eq} with the corresponding forcing:

$$ECS(R) = -\frac{R(2\times CO_2)}{\lambda_{eq}(R)} = \frac{R(2\times CO_2)}{R}\Delta T_{eq}(R). \tag{2}$$

Assessing ECS state-dependence, that is, the inconstancy of ECS(R), is important for warming projections under different levels of forcing. Assuming a constant ECS leads to incorrect warming estimates if the climate system is state dependent. State independence between $2\times CO_2$ and $4\times CO_2$ was assumed in the Coupled Model Intercomparison Project 5 (CMIP5): ECS($2\times CO_2$) was estimated as $\frac{1}{2}\Delta T_{eq}$, with ΔT_{eq} extrapolated from 150 year long $4\times CO_2$ simulations (Andrews et al., 2012, 2015; IPCC, 2013). Even disregarding extrapolation biases due to transient λ changes (Andrews et al., 2015; Geoffroy et al., 2013), these estimates for ECS($2\times CO_2$) may be biased if CMIP5 models are state dependent. This cannot be evaluated for the whole ensemble

because no 2×CO$_2$ experiment was included in CMIP5. The possibility of ECS state-dependence is only mentioned briefly in IPCC (2013), but there are some recent studies on the subject.

Most coupled general circulation models (GCMs) and slab ocean models exhibit ECS state-dependence to some degree. Some GCMs of earlier model generations show a decreasing ECS with increasing forcing (Colman & McAvaney, 2009; Stouffer & Manabe, 2003; Voss & Mikolajewicz, 2001). Comparing these results to simulations from the Community Climate System Model (CCSM3/CCSM4), Kutzbach et al. (2013) find a higher ECS under smaller-than-present forcings but no robust state-dependence under higher forcings. There is evidence from multimodel studies that state-of-the-art GCMs simulate an increasing climate sensitivity with increasing forcing (Good et al., 2015; Meraner et al., 2013). However, Good et al. (2015) only present 150 year temperatures without ECS extrapolations, and the analysis of Meraner et al. (2013) is complicated by the time scale inconsistency between scenarios. The multimodel findings are supported by the CCSM3 model, which exhibits the same ECS state-dependence in multimillennial simulations (Caballero & Huber, 2013; Jonko et al., 2013). On a century time scale, state-dependence is small to negligible in some models (Gregory et al., 2004; Hansen et al., 2005), even including models that exhibit substantial equilibrium state-dependence (Stouffer & Manabe, 2003; Voss & Mikolajewicz, 2001).

The causes of ECS state-dependence are model dependent. Notable state-dependence contributions are reported from the albedo feedback (e.g., Colman and McAvaney, 2009; Stouffer and Manabe, 2003), cloud and water vapor feedbacks (e.g., Jonko et al., 2013; Meraner et al., 2013), and CO$_2$ forcing (e.g., Caballero and Huber, 2013; Gregory et al., 2015).

Earth system models of intermediate complexity (EMICs) have not been systematically analyzed in terms of state-dependence. While some of the EMICs do not simulate some of the feedbacks that may be state dependent—for example, only about half of the EMICs included in IPCC (2013) feature interactive clouds (Eby et al., 2013)—most of them include ocean dynamics, snow and sea ice responses, and various radiative processes that may cause state-dependence. For example, the UVic and ECBilt-CLIO EMICs show a decreasing ECS with increasing CO$_2$ concentration (Knutti & Rugenstein, 2015; Weaver et al., 2007). Furthermore, EMICs are computationally inexpensive, enabling multimillennial full equilibrium simulations.

We analyze 2×CO$_2$ and 4×CO$_2$ stabilization experiments performed with an ensemble of 15 EMICs readily available from the EMIC-AR5 intercomparison (Eby et al., 2013). While the 1,000 year temperatures for the 2×CO$_2$ and 4×CO$_2$ simulations are listed in Eby et al. (2013) and IPCC (2013), they are not comparatively discussed. Furthermore, many EMICs are not in equilibrium after 1,000 years, and ECS estimates from extrapolation methods are missing. We compare ECS estimates from two commonly used extrapolation methods (Gregory et al., 2004; Steinacher & Joos, 2016) and investigate their state-dependence (sections 3.1 and 3.2). We perform additional simulations in one EMIC, the Bern3D-LPX model, to investigate the physical causes of its equilibrium and transient state-dependence (sections 3.3 and 3.4). We focus on positive forcings relevant for future projections, as state-dependence under colder conditions has been extensively studied (e.g., Colman and McAvaney, 2009; Friedrich et al., 2016; Köhler et al., 2015; Kutzbach et al., 2013; Lunt et al., 2010).
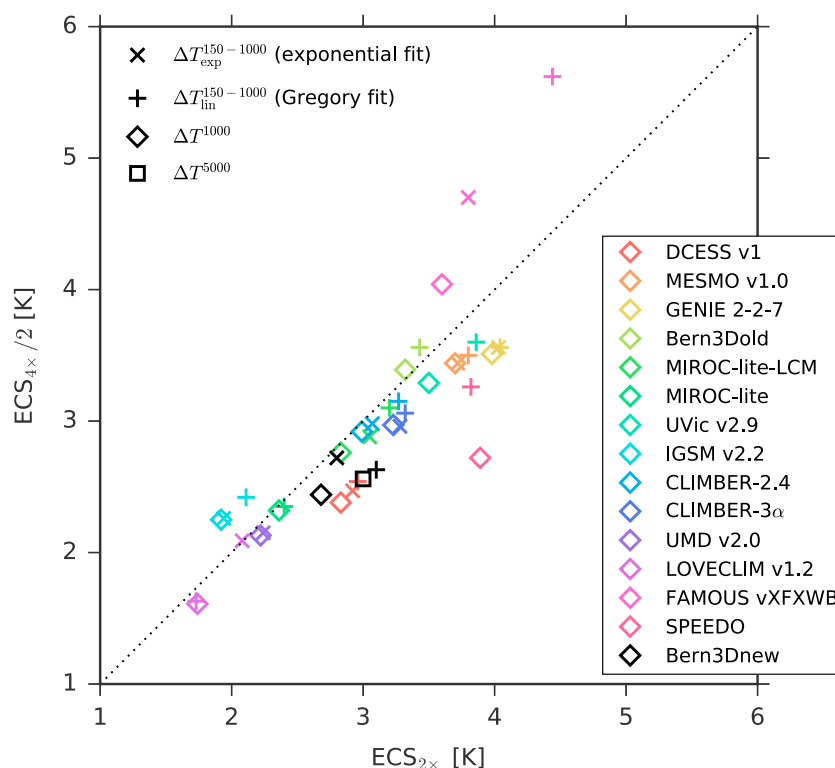
2. Methods

2.1. EMIC Ensemble Analysis
The EMIC-AR5 intercomparison (Eby et al., 2013) featured 15 EMICs, for which time series output of selected quantities is available from http://climate.uvic.ca/EMICAR5/results/ (hereafter EMIC-AR5). Models are listed in Figure 1 legend; see Table 1 in Eby et al. (2013) for descriptions and references. We exclude the IAP model because it has no 2×CO$_2$ simulation available on EMIC-AR5.

We use three EMIC-AR5 simulations: Experiment 4Xc where CO$_2$ increases by 1% per year and then stabilizes at 4 times the preindustrial concentration (hereafter 4×CO$_2$), the abrupt CO$_2$ doubling experiment 2X (hereafter 2×CO$_2$), and the control simulation H_CTR. We use the 1%/year quadrupling simulation instead of an abrupt quadrupling simulation to highlight potential difficulties when extrapolating ECS from this widely used idealized scenario (section 3.2 and supporting information section S2.2). This choice does not alter our findings on ECS state-dependence (section 3.2 and Table S1).

Temperature and heat uptake anomalies for the 2×CO$_2$ and 4×CO$_2$ simulations are calculated by subtracting the mean values of H_CTR from 2×CO$_2$ and 4×CO$_2$ time series. For three models, 4×CO$_2$ starts with temperature offsets compared to H_CTR, which cannot be attributed to forcing or variability. Therefore, an

Figure 1. ECS state-dependence in the EMIC-AR5 ensemble (Eby et al., 2013) and Bern3Dnew. Symbols indicate different ECS estimation methods (section 2.1). Colors correspond to different EMICs, listed in the legend roughly in order of ascending complexity.

additional temperature offset correction is applied to both 2×CO$_2$ and 4×CO$_2$ for these models (section S1). The correction amounts to +0.08°C for FAMOUS, −0.22°C for LOVECLIM, and +0.28°C for SPEEDO.

ECS is estimated from the anomaly time series using three different methods. The first estimate is obtained from averaging the last decade of the 1,000 year simulations (ΔT^{1000}), although some of the EMICs are not fully equilibrated by then. This estimate corresponds to Eby et al. (2013) apart from slight differences for the three corrected models. The second estimate ΔT_{lin} is obtained using the "Gregory method" (Gregory et al., 2004); the third estimate ΔT_{exp} is extrapolated from an exponential fit on three different time scales (Caldeira & Myhrvold, 2013; MacKay & Ko, 1997; Steinacher & Joos, 2016). $\Delta T_{\text{lin}}^{150-1000}$ and $\Delta T_{\text{exp}}^{150-1000}$ are consistently estimated from simulation years 150–1,000, because the forcing in 4×CO$_2$ is only constant after year 140. For 2×CO$_2$, an additional exponential estimate $\Delta T_{\text{exp}}^{1-1000}$ is obtained from the full time series, and a shorter Gregory estimate $\Delta T_{\text{lin}}^{20-150}$ from years 20–150, consistent with Andrews et al. (2015).

2.2. Sensitivity Tests in the Bern3D-LPX Model

To investigate the physical causes of ECS state-dependence, we perform additional simulations in the Bern3D-LPX model (Ritz et al., 2011; Stocker et al., 2014). We use an updated version (Roth et al., 2014) (hereafter Bern3Dnew) compared to the one used for EMIC-AR5 (hereafter Bern3Dold). The most important difference is an increased horizontal resolution mainly at high latitudes, which greatly improves the strength of the Antarctic Circumpolar Current (ACC) and results in a more stable Atlantic Meridional Overturning Circulation (AMOC). An Atlantic-to-Pacific freshwater flux correction (Zaucker et al., 1994) is no longer required, but a freshwater flux correction of −0.07 sverdrup (1 Sv = 10^6 m^{3}s^{-1}) is still applied in the Weddell Sea to locally enhance deep water formation.

With this model we perform the same 2×CO$_2$ and 4×CO$_2$ simulations as in EMIC-AR5, extended to 5,000 years. The 5,000 year temperature ΔT^{5000} of 2×CO$_2$ is the true ECS of the model and can be used as a benchmark for the other ECS estimation methods. To investigate ECS state for a larger range of forcings relevant for future projections, we perform additional 5,000 year simulations with abrupt CO$_2$ increases between 1.5×CO$_2$ (∼420 ppm) and 6×CO$_2$ (∼1670 ppm).

The simulations described above are run in the *standard* model configuration and six modified configurations to estimate state-dependence contributions of albedo, ocean mixing, and forcing. The first modified configuration features a different initial condition with a colder Southern Hemisphere (*colder SH*). This is achieved by reducing atmospheric heat transport diffusivity linearly with latitude from 33% on the South Pole to zero reduction on the North Pole. Southern high latitudes (>50°S) are about 3°C colder on average in the *colder SH* preindustrial simulation than in the standard preindustrial simulation, and sea ice extent is increased by about 30%. Perturbed CO_2 simulations in this setup continue with the same reduced atmospheric heat transport diffusivity.

Other modified configurations are restarted from the standard preindustrial simulation but with either albedo or ocean mixing held fixed to a preindustrial climatology. While such decoupling is unphysical with respect to the removed interaction, it is nevertheless helpful to assess the impact of albedo feedback and mixing changes on state-dependence. In *fixed α*, *fixed $α_{NH}$*, and *fixed $α_{SH}$*, the two-dimensional albedo field is fixed globally or only in one hemisphere, as denoted by the subscript. In *fixed mixing*, ocean mixing is kept constant, including advection, convection, and Gent-McWilliams mixing (Gent & McWilliams, 1990). This is achieved mainly by prescribing ocean density to a seasonally varying three-dimensional density field diagnosed from an unperturbed simulation year. Density is thereby decoupled from the evolving temperature and salinity, which still influence heat and freshwater fluxes in the ocean; only the volume transport is fixed. Furthermore, wind stress scaling with sea ice area is disabled to keep advection constant.

The final configuration *BG14 forcing* corresponds to the standard configuration apart from a different forcing calculation. Forcing is calculated according to Myhre et al. (1998) in the standard configuration:

$$R = 5.35 \text{Wm}^{-2} \cdot ln(C/C_0), \tag{3}$$

where C_0 and C are the preindustrial and perturbed CO_2 concentrations. In the *BG14 forcing* configuration; a more recent formula based on line-by-line integration of CO_2 absorption is employed (Byrne & Goldblatt, 2014):

$$R = 5.32 \text{Wm}^{-2} \cdot ln(C/C_0) + 0.39 \text{Wm}^{-2} \cdot ln(C/C_0)^2 \tag{4}$$

The *BG14 forcing* configuration thus explores how ECS state-dependence is influenced by forcing state-dependence, that is, by deviations from logarithmic CO_2 forcing.

3. Results

3.1. ECS State-Dependence in the EMIC Ensemble

Figure 1 compares ECS estimates from the 2×CO_2 and 4×CO_2 simulations; state-independent models would lie exactly on the diagonal. Some EMICs are nearly state independent: for example, five models (Bern3Dold, UMD, MIROC-lite, MIROC-lite-LCM, and CLIMBER-2.4) exhibit relative ECS changes of less than 5% between 2×CO_2 and 4×CO_2 across all ECS estimation methods. The other EMICs exhibit more substantial ECS state-dependence. This cannot be analyzed on the process level based on the available time series, but we compare model configurations to identify possible state-dependence contributions. No multimodel means are shown because the mean state-dependence depends on model selection, and extrapolated ECS estimates are not available for some models (section 3.2).

ECS decreases most strongly with forcing in Bern3Dnew, GENIE, DCESS, and SPEEDO, by 11–15% in the Gregory estimates. GENIE and MESMO have similar model configurations to Bern3Dnew (Eby et al., 2013); their similar state-dependence may therefore also be albedo-related (section 3.3). Contrarily, Bern3Dold is close to state independent with an opposite tendency to increasing sensitivity. This suggests that in EMICs of this kind (frictional geostrophic ocean and two-dimensional EBM), state-dependence is influenced by small differences in model configuration and initial conditions (section 3.3). On the other hand, DCESS is the lowest-complexity model of the ensemble and SPEEDO one of the most comprehensive, featuring an eight-layer atmosphere with interactive clouds. The processes causing state-dependence in these models may thus be different, involving unforced centennial variability in SPEEDO (section S2.3).

Only 2 out of 15 EMICs, FAMOUS and IGSM, show a substantially increased ECS with higher forcing. Both models feature 11-layer atmospheres with interactive clouds (zonally averaged in IGSM), so the processes

causing their state-dependence could be similar to those in the CCSM3 and ECHAM6 (Jonko et al., 2013; Meraner et al., 2013). However, two out of the other four EMICs featuring interactive clouds exhibit an opposite state-dependence (CLIMBER-3α and SPEEDO), and the remaining two are nearly state independent (CLIMBER2.4 and UMD). This spread underlines a high uncertainty in cloud feedback contributions to ECS state-dependence (Colman & McAvaney, 2009; Meraner et al., 2013).

At least 10 out of 14 EMICs from EMIC-AR5 use the Myhre et al. (1998) forcing, that is, a factor of 2 between 2×CO_2 and 4×CO_2 forcings. For three models, the forcing is not included in the EMIC-AR5 output (FA, GE, and SP); only for the I2 model, a nonlogarithmic forcing is specified ($R(4×CO_2) = 2.14 \cdot R(2×CO_2)$). This may contribute to I2's higher ECS under higher forcing (Caballero & Huber, 2013; Jonko et al., 2013).

3.2. Comparison of Different ECS Estimation Methods

All ECS estimates for the EMIC-AR5 ensemble and Bern3Dnew are listed in Table S1; the ones extrapolated from years 150–1,000 are also included in Figure 1. General findings are described below, with peculiarities of single models in section S2.3.

Both the exponential fit ($\Delta T_{\exp}^{150-1000}$) and the Gregory method ($\Delta T_{\lin}^{150-1000}$) yield higher ECS estimates than 1,000 year temperature (ΔT^{1000}) for most models (Figure 1). In the multimodel mean, $\Delta T_{\exp}^{150-1000}$ is 4% (6%) higher than ΔT^{1000} in 2×CO_2 (4×CO_2) and $\Delta T_{\lin}^{150-1000}$ is 8% (10%) higher (Table S1). The maximum difference found for single models amounts to 20% in 2×CO_2 (LOVECLIM, $\Delta T_{\exp}^{150-1000}$) and 37% in 4×$CO_2$ (FAMOUS, $\Delta T_{\lin}^{150-1000}$). Equilibration is thus lower in 4×CO_2, and differences between estimation methods are comparable in magnitude to ECS state-dependence (section 3.1).

Many EMICs still have a substantial radiative imbalance ($N > 0$) after 1,000 years, which is generally stronger in 4×CO_2 (Figure S1). For those models, the Gregory method ($\Delta T_{\lin}^{150-1000}$) yields higher ECS estimates than the exponential fits ($\Delta T_{\exp}^{150-1000}$). $\Delta T_{\lin}^{150-1000}$ is an accurate ECS estimate if the feedback parameter λ does not change substantially from years 150–1,000 to equilibrium. In this case, the lower $\Delta T_{\exp}^{150-1000}$ would underestimate ECS. This is likely true for most EMICs as λ is close to constant over the first 1,000 simulation years (Figure S1), but longer simulations are needed to confirm this.

Only in three EMICs is λ substantially time dependent (Bern3Dnew, LOVECLIM, and SPEEDO, section S2.4). This explains the difference between $\Delta T_{\lin}^{20-150}$ and $\Delta T_{\lin}^{150-1000}$ in those models, as well as the slight ECS overestimation by $\Delta T_{\lin}^{150-1000}$ in Bern3Dnew. In Bern3Dnew and LOVECLIM, the slope $-\lambda$ decreases with time like in most GCMs (Andrews et al., 2015; Geoffroy et al., 2013). In SPEEDO, $-\lambda$ increases due to centennial variability.

The multiexponential fit of 2×CO_2 is sensitive to the selected time interval in some EMICs. The shorter interval ($\Delta T_{\exp}^{150-1000}$) yields some unusable fits (section S2.3). This suggests that the multiexponential fit is generally only appropriate for the response to abrupt forcing, and only if the fast response is included ($\Delta T_{\exp}^{1-1000}$). However, for most EMICs both time scales yield similar results. The exponential fit is inappropriate for temperature evolutions with slow variability, such as SPEEDO's centennial oscillations (section S2.3). These are handled better by the less shape-sensitive Gregory fit.

ECS state-dependence is poorly represented by $\Delta T_{\exp}^{150-1000}$ for Bern3Dnew; otherwise, state-dependence is mostly similar across estimation methods (Figure 1). For Bern3Dnew, the relative difference between 2×CO_2 and 4×CO_2 is smaller in ΔT^{1000} than in ΔT^{5000}. This indicates that the ECS state-dependence is not yet fully developed after 1,000 years, in qualitative agreement with Voss and Mikolajewicz (2001) and Stouffer and Manabe (2003) (section 3.4). Conversely, in SPEEDO the relative difference is larger in ΔT^{1000} than in $\Delta T_{\lin}^{150-1000}$. This is because 4×$CO_2$ is less equilibrated than 2×CO_2 after 1,000 years (Figure S1), such that its extrapolated subsequent warming is larger.

The ECS estimates ΔT^{1000} and $\Delta T_{\lin}^{150-1000}$ from the abrupt 4×CO_2 simulation are very similar to those from the 1%/year simulation (Table S1). $\Delta T_{\exp}^{150-1000}$ differs more notably for some models, but state-dependence is qualitatively consistent. This calls for caution when using exponential extrapolation for nonabrupt scenarios (section S2.2) but indicates robustness of the Gregory estimates and our state-dependence results.

3.3. ECS State-Dependence in the Bern3D-LPX Model

The ECS state-dependence of the Bern3Dnew model is mainly due the state-dependent sea ice-albedo feedback in the Southern Ocean (Figure 2). This is identified using modified model configurations (section 2.2). In the absence of albedo feedback, there is no ECS state-dependence in Bern3Dnew (*fixed* α). The northern hemispheric albedo feedback (active in *fixed* α_{SH}) is also virtually state independent. The ECS state-dependence
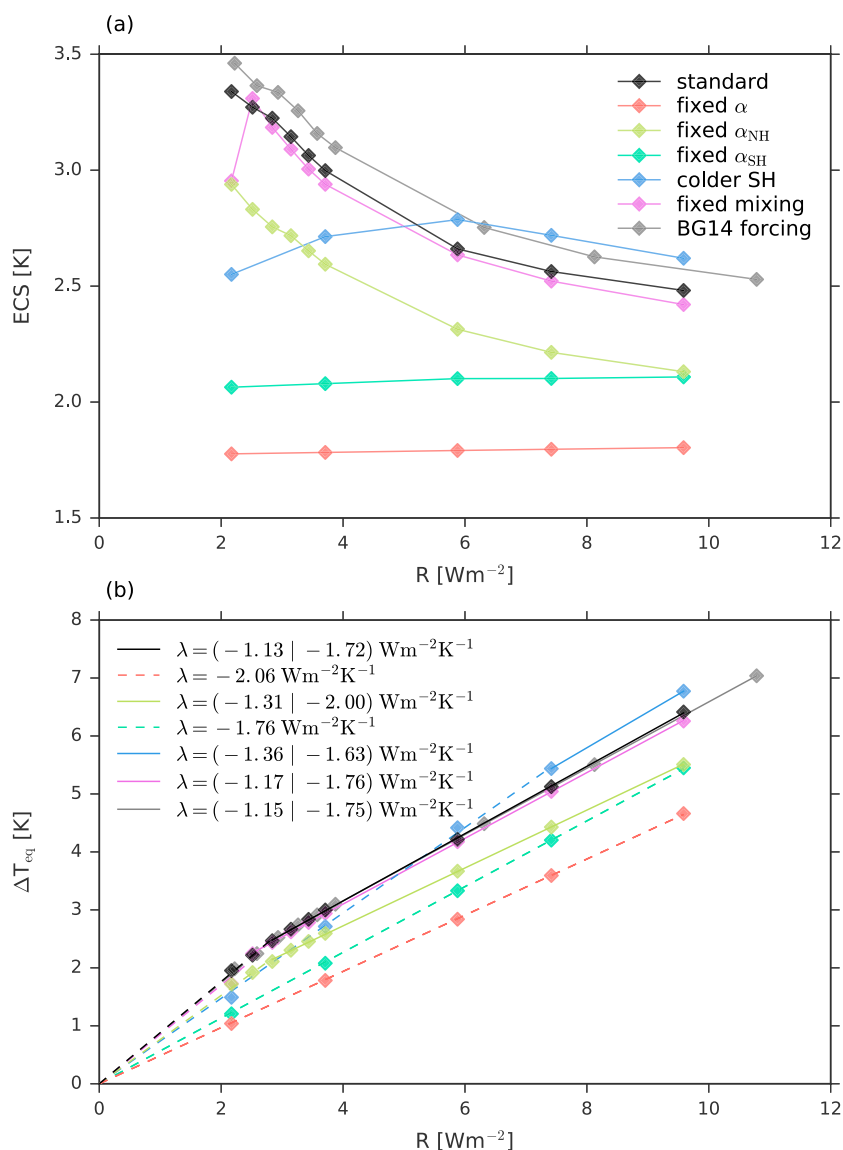
Figure 2. State-dependence of (a) ECS and (b) ΔT_{eq} in the Bern3Dnew model. Colors indicate different model configurations (section 2.2). Diamonds show model output, lines in Figure 2b show linear fits. Solid lines only include states where Southern Ocean sea ice has melted to less than 10% of its preindustial value; dashed lines include all other values. Feedback parameters are given in the legend for small and large forcings to the left and right of the vertical dash.

is therefore caused by the southern hemispheric albedo feedback. This feedback is active in *fixed α_{NH}*, which shows qualitatively the same state-dependence as the fully coupled standard model configuration. The constant sensitivity offset is due to the lack of northern hemispheric albedo feedback. The state-dependence corresponds to a weakening of the southern hemispheric albedo feedback due to the diminishing sea ice extent, as described below.

The state-dependence of the scaled ECS following equation (2) (Figure 2a) can be well approximated by a roughly bilinear state-dependence of ΔT_{eq} (Figure 2b). The slope of the first near-linear phase is mainly determined by the amount of Southern Ocean sea ice melt per unit forcing. The second phase begins at the forcing where Southern Ocean sea ice has melted to less than 10% of its preindustrial extent, such that no substantial ice-albedo feedback remains. The slope of this phase is determined by the remaining feedbacks and is therefore similar in all available configurations ($\lambda = -1.72 / -1.76 / -1.63$ Wm^{-2} K^{-1}) to the state-independent slope of *fixed α_{SH}* ($\lambda = -1.77$ Wm^{-2} K^{-1}). The smaller slope ($\lambda = -2.00$ Wm^{-2} K^{-1}) in *fixed α_{NH}* is explained by

the lack of northern hemispheric albedo feedback. It is thus similar to the state-independent slope of *fixed α* ($\lambda = -2.06\,\mathrm{Wm^{-2}\,K^{-1}}$).

The slighter and partly opposite ECS state-dependence in the *colder SH* configuration is also due to changes in the southern high-latitude albedo feedback. ECS increases slightly with increasing forcing between $1.5\times CO_2$ and $3\times CO_2$. While the sea ice extent always decreases with forcing, the albedo feedback is not necessarily reduced as long as enough sea ice is available for melting. Here the feedback increases slightly, because the southern sea ice loss per unit warming (section 3.4) increases with forcing, indicating nonlinear melting depending on the affected sea ice regions. ECS decreases between $3\times CO_2$ and $6\times CO_2$, where the ice melts completely even in *colder SH*. In agreement with Bern3Dold, ECS($4\times CO_2$) is slightly higher than ECS($2\times CO_2$). These results show that the albedo-induced ECS state-dependence is strongly influenced by model configuration and initial conditions, mostly by the availability and sensitivity of Southern Ocean sea ice. This state-dependence contribution is therefore tuneable in the Bern3D-LPX and similar EMICs.

Fixing ocean mixing has little influence on equilibrium state-dependence (Figure 2), except for an ECS jump from $1.5\times CO_2$ to $1.6\times CO_2$. This exception is due to an unphysical acceleration of sea ice melting in a region of fixed convection, which is only triggered for forcings of $1.6\times CO_2$ or higher. This effect will be described in a future study. However, ocean mixing strongly influences transient state-dependence (section 3.4).

The *BG14 forcing* configuration reveals that forcing state-dependence cannot counteract the albedo-induced ECS state-dependence. This is because the additional warming caused by higher forcing further weakens the ice-albedo feedback. The near-constant offset between *BG14 forcing* and *standard* stems from the higher $R(2 \times CO_2)$ under *BG14 forcing* (equation (2)). While $\Delta T_{eq}(R)/R$ for high forcings is decreased compared to *standard* due to state-dependence, this decrease is much smaller than the increase in $R(2 \times CO_2)$.

The equivalence of state-dependence and forcing dependence of ECS in Bern3Dnew is confirmed by additional standard experiments starting from different initial states (section S3.1 and Figure S5).

3.4. Bern3D-LPX State-Dependence of Transient Climate Sensitivity

Transient state-dependence of temperature and feedback can differ from equilibrium state-dependence. In the Bern3Dnew model, temperature state-dependence becomes evident after roughly 400 years between $2\times CO_2$ and $4\times CO_2$ and after roughly 1,000 years between $1.5\times CO_2$ and $2\times CO_2$ (Figure 3a). We investigate this using a diagnostic latitudinal EBM (e.g., Rose and Rayborn, 2016) to calculate local feedbacks λ_{loc}:

$$R - \Delta N(\theta, t) - \Delta(\nabla \cdot \mathbf{F})(\theta, t) = -\lambda_{loc}(\theta, t)\Delta T(\theta, t), \qquad (5)$$

where $-\Delta(\nabla \cdot \mathbf{F})(\theta, t)$ is the change in meridional heat flux convergence at latitude θ and time t. The meridional heat flux $\mathbf{F}$ consists of oceanic and atmospheric heat transport. All quantities are zonal means, and R is uniform.

Like equilibrium state-dependence (section 3.3), transient state-dependence is dominated by sea ice melting in the southern high latitudes. Therefore, we focus on this region in Figure 3. We highlight the transient influence of ocean dynamics by comparing the *standard* model configuration (Figures 3a, 3c, 3e, and 3g) to the configuration with fixed ocean mixing (*fixed mixing*, Figures 3b, 3d, 3f, and 3h). In *standard*, the Southern Ocean Meridional Overturning Circulation (SOMOC) decreases mainly due to the sea surface density decrease from sea ice melting, which is stronger for higher forcing (Figure 3g).

Both in *standard* and *fixed mixing*, the global temperature sensitivity (Figures 3a and 3b) is broadly in line with the southern high-latitute feedback $\lambda_{loc}(40-90°S)$ (Figures 3c and 3d). This is because changes in the global feedback are dominantly driven by changes in $\lambda_{loc}(40-90°S)$. The exception to this are variations in $\lambda_{loc}(40-90°S)$ in standard during the first 400 years (Figure 3c), which are roughly compensated in the rest of the world (not shown).

The changes in $\lambda_{loc}(40-90°S)$ are essentially determined by the southern sea ice area loss (Figures 3e and 3f) per unit warming, $\Delta a_{ice}(40-90°S)\Delta T$. This is because the albedo feedback is $\lambda_\alpha \approx K_\alpha \Delta\alpha/\Delta T$, where K_α is the radiative kernel (Soden et al., 2008), and $\Delta\alpha/\Delta T$ is driven by $\Delta a_{ice}(40-90°S)\Delta T$. ECS in $4\times CO_2$ is lower than in $2\times CO_2$ because $\Delta a_{ice}(40-90°S)$ is the same in both simulations (complete meltdown), but ΔT is higher in $4\times CO_2$. In other words, $4\times CO_2$ has more excess warming occurring at lower feedback after all Southern Ocean ice is melted away (section 3.3). This applies to both *standard* and *fixed mixing*, but their transient sensitivities differ strongly.
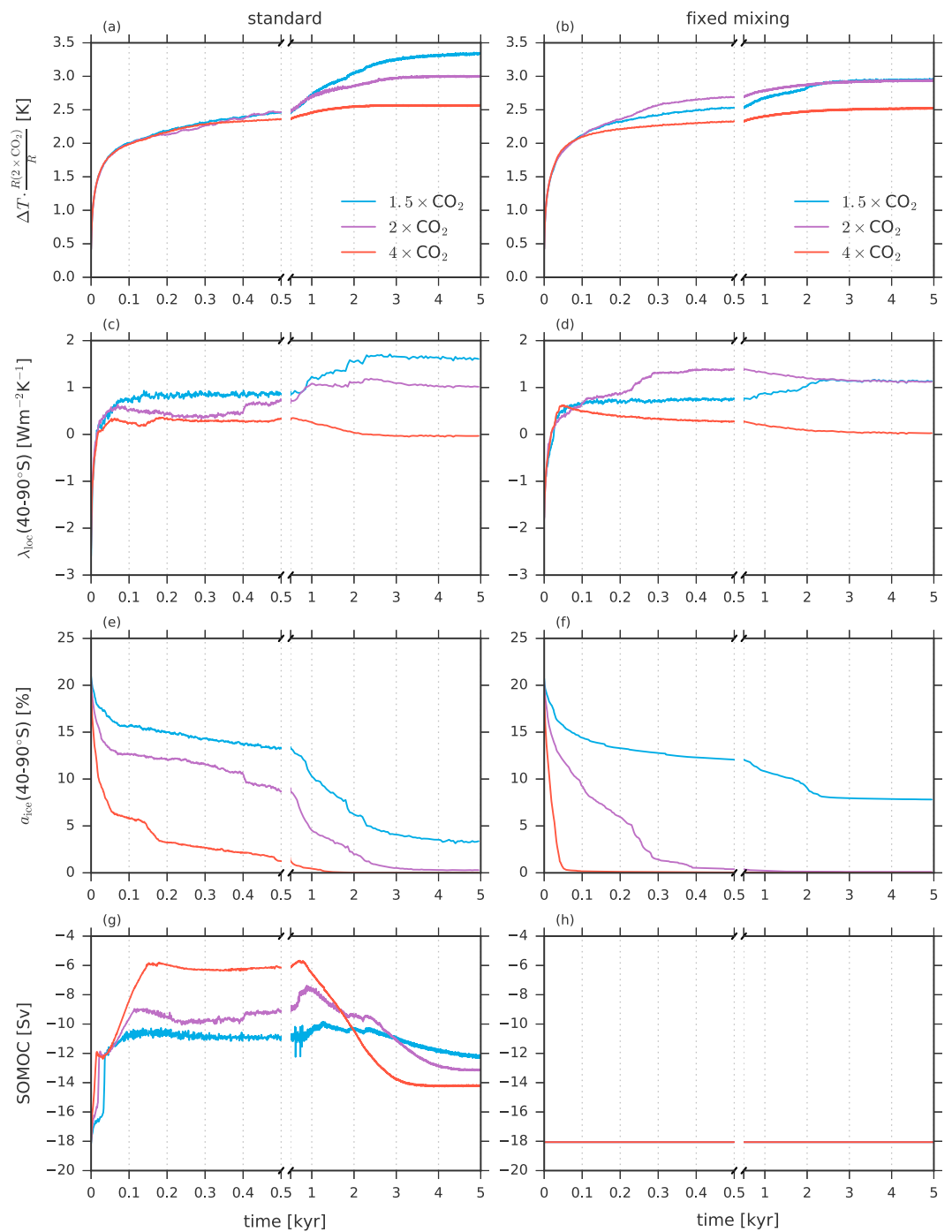
Figure 3. Transient state-dependence in the Bern3Dnew model. Colors indicate different levels of abrupt CO_2 forcing, in the (a, c, e, g) *standard* and (b, d, f, h) *fixed mixing* model configurations (section 2.2). Variables: global mean ΔT scaled to $2 \times CO_2$, local feedback and ice area averaged over 40–90°S, and Southern Ocean Meridional Overturning Circulation (SOMOC).

The rapid SOMOC weakening and convective adjustments in *standard* cause a slower high-latitude SST increase, delaying sea ice melting substantially. A near-complete loss of Southern Ocean sea ice is realized after 100 years in $4 \times CO_2$ in *fixed mixing*, but more than 1,000 years later in *standard*. The ocean mixing-induced delay is even larger for $2 \times CO_2$.

The state-dependence between $1.5 \times CO_2$ and $2 \times CO_2$ differs both transiently and in equilibrium between *standard* and *fixed mixing*. In *fixed mixing*, $2 \times CO_2$ is more sensitive than $1.5 \times CO_2$ during years 200–2,000,

because of a rapid convection-induced meltdown during years 200–400 in $2\times CO_2$. The $1.5\times CO_2$ only catches up on melting per unit warming between years 500 and 2,000, eventually reaching the same ECS as $2\times CO_2$. In *standard*, the $1.5\times CO_2$ and $2\times CO_2$ transient sensitivities are nearly identical for 1,000 years, because differences in $\lambda_{loc}(40-90°N)$ are small during years 400–1,000 and counteracted by other regions in earlier years. During equilibration in years 1,000–5,000, climate sensitivity in $1.5\times CO_2$ becomes larger than in $2\times CO_2$, because of a larger a_{ice} loss. This is because ECS of $2\times CO_2$ is already limited by the lack of available Southern Ocean sea ice (section 3.3).

In summary, we find a time of emergence of roughly 100 to 1,000 years for the state-dependence of climate sensitivity, depending on model configuration and forcing difference. Here we do not refer to the statistical definition of the time of emergence of climate signals (Hawkins & Sutton, 2012) related to achieving a sufficient signal-to-noise ratio. We refer to the time scale at which state-dependence becomes evident by surpassing counteracting physical effects. In the case of sea ice albedo-driven state-dependence, the dominant such effects are ocean mixing adjustments, which delay the emergence of state-dependence between $2\times CO_2$ and $4\times CO_2$ by roughly 300 years. We conclude that the ECS state-dependence of any coupled model including slow ocean processes may not be detectable from too short simulations. Our model suggests that at least 500 simulation years are required to identify state-dependence between $2\times CO_2$ and $4\times CO_2$, but the time of emergence of state-dependence may differ for other models.

4. Summary and Conclusions

With increased forcing, ECS decreases in 12 out of 15 analyzed EMICs and increases in the remaining three. Some of these changes are small enough to be regarded as state independent; for example, five models have sensitivity changes smaller than 5%. Due to the strongly varying model complexity across the ensemble, the causes of state-dependence may be manifold. An important driver of decreasing sensitivity with higher forcing is the albedo feedback (Jonko et al., 2013; Kutzbach et al., 2013; Stouffer & Manabe, 2003), which is simulated by all EMICs. We show that this feedback is the main cause of ECS state-dependence in the new version of the Bern3D-LPX model. The ECS decreases with increasing forcing from $1.5\times CO_2$ to $6\times CO_2$ due to the diminishing availability of Southern Ocean sea ice. For a model configuration with a colder Southern Hemisphere, an opposite and much less substantial ECS state-dependence is simulated. This indicates that the albedo-related contribution to state-dependence is tuneable by simple changes in model configuration or initial state.

Differences between ECS estimation methods are of comparable magnitude to ECS state-dependence. Many EMICs are not in equilibrium 1,000 years after a perturbation; estimating their ECS thus requires extrapolation. For the year 150–1000 time interval, we suggest that the Gregory method (Gregory et al., 2004) produces more reliable results than a multiexponential extrapolation (e.g., MacKay and Ko, 1997), but longer simulations are required to confirm this.

The ECS decrease with increasing forcing simulated by most EMICs is mainly in agreement with older GCMs (Colman & McAvaney, 2009; Stouffer & Manabe, 2003; Voss & Mikolajewicz, 2001). It is contrary to growing evidence from state-of-the-art GCMs that ECS increases with increasing forcing (Caballero & Huber, 2013; Good et al., 2015; Jonko et al., 2013; Meraner et al., 2013). This discrepancy cannot clearly be attributed to a lack of cloud feedbacks in the EMICs, as only two out of six EMICs that feature interactive clouds show an increasing sensitivity in line with GCMs.

Most EMICs use logarithmic CO_2 forcing (Myhre et al., 1998), in contrast to GCMs that account for a stronger-than-logarithmic forcing increase for higher CO_2 concentrations (Caballero & Huber, 2013; Gregory et al., 2015). Part of the discrepancy in ECS state-dependence between EMICs and GCMs may thus be resolved if the Byrne and Goldblatt (2014) CO_2 forcing is implemented in EMICs. However, our Bern3D-LPX simulations show that albedo-driven state-dependence cannot be counteracted by forcing state-dependence.

The GCM results are not yet conclusive because many GCMs lack simulations with different levels of abrupt forcing. This gap will be filled by two ongoing model intercomparison projects: nonlinMIP (Good et al., 2016) and longRunMIP (www.longrunmip.org). Our results show that ECS state-dependence may not be detectable for hundreds of simulation years, due to transient counteracting effects such as ocean mixing adjustments. Therefore, CMIP6 modeling groups should be motivated to participate in longrunMIP and to carry out the nonessential extensions of the $2\times CO_2$ and $4\times CO_2$ experiments in nonlinMIP (Good et al., 2016). If the results

from these MIPs confirm a robustly increasing ECS with forcing, EMIC modeling groups may have to include or adjust relevant feedback parametrizations to reproduce this opposite state-dependence, in order to preserve the status of the EMICs as valuable tools for long-term projections and sensitivity studies.

References

Andrews, T., Gregory, J. M., & Webb, M. J. (2015). The dependence of radiative forcing and feedback on evolving patterns of surface temperature change in climate models. *Journal of Climate*, *28*(4), 1630–1648. https://doi.org/10.1175/JCLI-D-14-00545.1

Andrews, T., Gregory, J. M., Webb, M. J., & Taylor, K. E. (2012). Forcing, feedbacks and climate sensitivity in CMIP5 coupled atmosphere-ocean climate models. *Geophysical Research Letters*, *39*, L09712. https://doi.org/10.1029/2012GL051607

Armour, K. C., Bitz, C. M., & Roe, G. H. (2013). Time-varying climate sensitivity from regional feedbacks. *Journal of Climate*, *26*(13), 4518–4534. https://doi.org/10.1175/JCLI-D-12-00544.1

Byrne, B., & Goldblatt, C. (2014). Radiative forcing at high concentrations of well-mixed greenhouse gases. *Geophysical Research Letters*, *41*, 152–160. https://doi.org/10.1002/2013GL058456

Caballero, R., & Huber, M. (2013). State-dependent climate sensitivity in past warm climates and its implications for future climate projections. *Proceedings of the National Academy of Sciences of the United States of America*, *110*(35), 14,162–14,167. https://doi.org/10.1073/pnas.1303365110

Caldeira, K., & Myhrvold, N. P. (2013). Projections of the pace of warming following an abrupt increase in atmospheric carbon dioxide concentration. *Environmental Research Letters*, *034039*(3). https://doi.org/10.1088/1748-9326/8/3/034039

Charney, J. G., Arakawa, A., Baker, D. J., Bolin, B., Dickinson, R. E., Goody, R. M., . . . Wunsch, C. I. (1979). *Carbon dioxide and climate: A scientific assessment*. Washington, DC: National Academy of Sciences.

Colman, R., & McAvaney, B. (2009). Climate feedbacks under a very broad range of forcing. *Geophysical Research Letters*, *36*, L01702. https://doi.org/10.1029/2008GL036268

Eby, M., Weaver, A. J., Alexander, K., Zickfeld, K., Abe-Ouchi, A., Cimatoribus, A. A., . . . Zhao, F. (2013). Historical and idealized climate model experiments: An intercomparison of Earth system models of intermediate complexity. *Climate of the Past*, *9*(3), 1111–1140. https://doi.org/10.5194/cp-9-1111-2013

Friedrich, T., Timmermann, A., Tigchelaar, M., Elison Timm, O., & Ganopolski, A. (2016). Nonlinear climate sensitivity and its implications for future greenhouse warming. *Science of Advanced*, *2*(11), E1501923. https://doi.org/10.1126/sciadv.1501923

Gent, P. R., & McWilliams, J. C. (1990). Isopycnal mixing in ocean circulation models. *Journal of Physical Oceanography*, *20*(1), 150–155. https://doi.org/10.1175/1520-0485(1990)020<0150:IMIOCM>2.0.CO;2

Geoffroy, O., Saint-Martin, D., Bellon, G., Voldoire, A., Olivie, D. J. L., & Tyteca, S. (2013). Transient climate response in a two-layer energy-balance model. Part II: Representation of the efficacy of deep-ocean heat uptake and validation for CMIP5 AOGCMs. *Journal of Climate*, *26*(6), 1859–1876. https://doi.org/10.1175/JCLI-D-12-00196.1

Good, P., Andrews, T., Chadwick, R., Dufresne, J.-L., Gregory, J. M., Lowe, J. A., . . . Shiogama, H. (2016). nonlinMIP contribution to CMIP6: Model intercomparison project for non-linear mechanisms: Physical basis, experimental design and analysis principles (v1.0). *Geoscientific Model Development*, *11*(9), 4019–4028. https://doi.org/10.5194/gmd-9-4019-2016

Good, P., Lowe, J. A., Andrews, T., Wiltshire, A., Chadwick, R., Ridley, J. K., . . . Shiogama, H. (2015). Nonlinear regional warming with increasing CO_2 concentrations. *Natural Climate Change*, *5*(2), 138–142. https://doi.org/10.1038/NCLIMATE2498

Gregory, J. M., Andrews, T., & Good, P. (2015). The inconstancy of the transient climate response parameter under increasing CO_2. *Philosophical Transactions of the Royal Society of London, Series A: Mathematical, Physical and Engineering Sciences*, *373*(2054), 20140417. https://doi.org/10.1098/rsta.2014.0417

Gregory, J. M., Ingram, W. J., Palmer, M. A., Jones, G. S., Stott, P. A., Thorpe, R. B., . . . Williams, K. D. (2004). A new method for diagnosing radiative forcing and climate sensitivity. *Geophysical Research Letters*, *31*, L03205. https://doi.org/10.1029/2003GL018747

Hansen, J., Sato, M., Ruedy, R., Nazarenko, L., Lacis, A., Schmidt, G. A., . . . Zhang, S. (2005). Efficacy of climate forcings. *Journal of Geophysical Research*, *110*, D18104. https://doi.org/10.1029/2005JD005776

Hawkins, E., & Sutton, R. (2012). Time of emergence of climate signals. *Geophysical Research Letters*, *39*, L01702. https://doi.org/10.1029/2011GL050087

IPCC (2013). *Climate change 2013: The physical science basis. Contribution of Working Group I to the Fifth Assessment Report of the Intergovernmental Panel on Climate Change*. Stocker, T. F. et al. (Eds.) 1535 pp., Cambridge, UK: Cambridge University Press. https://doi.org/10.1017/CBO9781107415324

Jonko, A. K., Shell, K. M., Sanderson, B. M., & Danabasoglu, G. (2013). Climate feedbacks in CCSM3 under changing CO_2 forcing. Part II: Variation of climate feedbacks and sensitivity with forcing. *Journal of Climate*, *26*(9), 2784–2795. https://doi.org/10.1175/JCLI-D-12-00479.1

Knutti, R., & Rugenstein, M. A. A. (2015). Feedbacks, climate sensitivity and the limits of linear models. *Philosophical Transactions of the Royal Society of London, Series A: Mathematical, Physical and Engineering Sciences*, *373*(2054). https://doi.org/10.1098/rsta.2015.0146

Köhler, P., de Boer, B., von der Heydt, A. S., Stap, L. B., & van de Wal, R. S. W. (2015). On the state dependency of the equilibrium climate sensitivity during the last 5 million years. *Climate of the Past*, *11*(12), 1801–1823. https://doi.org/10.5194/cp-11-1801-2015

Kutzbach, J. E., He, F., Vavrus, S. J., & Ruddiman, W. F. (2013). The dependence of equilibrium climate sensitivity on climate state: Applications to studies of climates colder than present. *Geophysical Research Letters*, *40*(14), 3721–3726. https://doi.org/10.1002/grl.50724

Lunt, D. J., Haywood, A. M., Schmidt, G. A., Salzmann, U., Valdes, P. J., & Dowsett, H. J. (2010). Earth system sensitivity inferred from Pliocene modelling and data. *Nature Geoscience*, *3*(1), 60–64. https://doi.org/10.1038/NGEO706

MacKay, R. M., & Ko, M. K. W. (1997). Normal modes and the transient response of the climate system. *Geophysical Research Letters*, *24*(5), 559–562. https://doi.org/10.1029/97GL00286

Meraner, K., Mauritsen, T., & Voigt, A. (2013). Robust increase in equilibrium climate sensitivity under global warming. *Geophysical Research Letters*, *40*(22), 5944–5948. https://doi.org/10.1002/2013GL058118

Myhre, G., Highwood, E. J., Shine, K. P., & Stordal, F. (1998). New estimates of radiative forcing due to well mixed greenhouse gases. *Geophysical Research Letters*, *25*(14), 2715–2718. https://doi.org/10.1029/98GL01908

Ritz, S. P., Stocker, T. F., & Joos, F. (2011). A coupled dynamical ocean-energy balance atmosphere model for paleoclimate studies. *Journal of Climate*, *24*(2), 349–375. https://doi.org/10.1175/2010JCLI3351.1

Rose, B. E. J., & Rayborn, L. (2016). The effects of ocean heat uptake on transient climate sensitivity. *Current Climate Change Reports*, *2*(4), 190–201. https://doi.org/10.1007/s40641-016-0048-4

Roth, R., Ritz, S. P., & Joos, F. (2014). Burial-nutrient feedbacks amplify the sensitivity of atmospheric carbon dioxide to changes in organic matter remineralisation. *Earth System Dynamics*, *5*(2), 321–343. https://doi.org/10.5194/esd-5-321-2014

Soden, B. J., Held, I. M., Colman, R., Shell, K. M., Kiehl, J. T., & Shields, C. A. (2008). Quantifying climate feedbacks using radiative kernels. *Journal of Climate*, *21*, 3504–3520. https://doi.org/10.1175/2007JCLI2110.1

Steinacher, M., & Joos, F. (2016). Transient Earth system responses to cumulative carbon dioxide emissions: Linearities, uncertainties, and probabilities in an observation-constrained model ensemble. *Biogeosciences*, *13*(4), 1071–1103. https://doi.org/10.5194/bg-13-1071-2016

Stocker, B. D., Feissli, F., Strassmann, K. M., Spahni, R., & Joos, F. (2014). Past and future carbon fluxes from land use change, shifting cultivation and wood harvest. *Tellus B*, *66*(1), 23188. https://doi.org/10.3402/tellusb.v66.23188

Stouffer, R. J., & Manabe, S. (2003). Equilibrium response of thermohaline circulation to large changes in atmospheric CO_2 concentration. *Climate Dynamics*, *20*(7), 759–773. https://doi.org/10.1007/s00382-002-0302-4

Voss, R., & Mikolajewicz, U. (2001). Long-term climate changes due to increased CO_2 concentration in the coupled atmosphere-ocean general circulation model ECHAM3/LSG. *Climate Dynamics*, *17*(1), 45–60. https: //doi.org/10.1007/PL00007925

Weaver, A. J., Eby, M., Kienast, M., & Saenko, O. A. (2007). Response of the Atlantic meridional overturning circulation to increasing atmospheric CO_2: Sensitivity to mean climate state. *Geophysical Research Letters*, *34*(5), L05708. https://doi.org/10.1029/2006GL028756

Winton, M., Takahashi, K., & Held, I. M. (2010). Importance of ocean heat uptake efficacy to transient climate change. *Journal of Climate*, *23*(9), 2333–2344. https://doi.org/10.1175/2009JCLI3139.1

Zaucker, F., Stocker, T. F., & Broecker, W. S. (1994). Atmospheric fresh-water fluxes and their effect on the global thermohaline circulation. *Journal of Geophysical Research*, *99*(C6), 12,443–12,457. https://doi.org/10.1029/94JC00526